Debiasing Welch's Method for Spectral Density Estimation

Lachlan C. Astfalck[1,2], Adam M. Sykulski[3], and Edward J. Cripps[1]

Abstract

Welch's method provides an estimator of the power spectral density that is statistically consistent. This is achieved by averaging over periodograms calculated from overlapping segments of a time series. For a finite length time series, while the variance of the estimator decreases as the number of segments increase, the magnitude of the estimator's bias increases: a bias-variance trade-off ensues when setting the segment number. We address this issue by providing a a novel method for debiasing Welch's method which maintains the computational complexity and asymptotic consistency, and leads to improved finite-sample performance. Theoretical results are given for fourth-order stationary processes with finite fourth-order moments and absolutely continuous fourth-order cumulant spectrum. The significant bias reduction is demonstrated with numerical simulation and an application to real-world data, where several empirical metrics indicate our debiased estimator compares favourably to Welch's. Our estimator also permits irregular spacing over frequency and we demonstrate how this may be employed for signal compression and further variance reduction. Code accompanying this work is available in the R and `python` languages.

Keywords: Welch's method; bias reduction; tapering; non-parametric estimation; periodogram.

1 Introduction

The periodogram is the fundamental non-parametric estimator of the power spectral density; however, it suffers from two deficiencies: the periodogram is statistically inconsistent and is biased with finite samples. By averaging multiple periodograms calculated from partitioned or overlapping segments of a time series, Welch (1967) overcomes the issue of inconsistency to provide a statistically consistent estimator of the power spectral density, eponymously known as Welch's estimator. Welch's estimator is simple to implement and easy to understand: all reasons that has led to its ubiquity in the applied sciences. However, for finite length time series, the issue of bias remains. Each segment's periodogram is biased and Welch's estimator inherits this bias. Further, as the magnitude of the bias is inversely related to the length of the segments, there is the classical inverse relationship between bias and variance of the estimator; this leads to the undesirable property that we become increasingly more certain in an estimator that is increasingly more biased. In this paper, we introduce a debiased analogue to Welch's estimator that we entitle the debiased Welch estimator.

Historically, a number of methodologies have been developed to mitigate the effects of bias. One such methodology is tapering (Thomson, 1982), where a taper is applied to the data; although, typically this reduces correlation between distant frequencies at the cost of increasing correlation between nearby frequencies, and so bias remains. More recently, Sykulski et al. (2019) provided methodology to debias spectral density estimates, but this methodology relies on the availability of the parametric form of the

---

[1] School of Physics, Mathematics & Computing, The University of Western Australia, 35 Stirling Hwy, Crawley, Australia

[2] Oceans' Graduate School, The University of Western Australia, 35 Stirling Hwy, Crawley, Australia

[3] Department of Mathematics, Imperial College London, South Kensington, London SW7 2BX, U.K.

power spectral density. In this paper, we extend the results in Sykulski et al. (2019) to non-parameteric estimation by constructing a natural basis representation to the power spectral density. From this basis representation we intentionally bias the bases, fit the biased bases to a biased estimate of the power spectral density, and recover debiased coefficients that are used to form our debiased non-parametric estimator. Tapering is ubiquitous in the applied sciences and augments both parametric and non-parametric estimation of the power spectral density, hence our method is developed to be applicable with any choice of taper.

Novel insight is provided across two theorems. The first presents theoretical results that make explicit how the properties of Welch's estimator are a function of the number of observations, number of segments, and the segment lengths. This theorem makes the finite sample bias explicit and motivates the construction of a new debiased alternative which we propose via a basis representation. To obtain a good representation of the power spectral density, however, we must specify a large number of basis functions and so estimation of the coefficients via direct optimisation of the Whittle likelihood, as in Sykulski et al. (2019), becomes computationally infeasible. The major contribution of this work is therefore housed in the second theorem, where we introduce methodology that leverages results established in the first theorem, to provide asymptotic results that enable fast and direct computation of the debiased Welch estimator. We build theory for time series requiring fourth-order stationarity with finite fourth-order moments and absolutely continuous fourth-order cumulant spectrum. The theory is established for all tapers, subject to the standard conditions of squared summability of the tapering sequence, thereby extending many classical results that use the raw periodogram, for example, those in Anderson (1971), Brillinger (1975) and Katznelson (1968).

The theoretical developments are also demonstrated by simulation. First, we use a canonical auto-regressive model of order four studied throughout the spectral estimation literature, see for example Percival et al. (1993). We use this model to contrast the performance of the standard and debiased Welch estimators as a function of the number of segments and the segment length. Next, we demonstrate the debiased Welch estimator in a real-world case study of coastal wave measurements. Here, we provide an example of where parametric methods struggle to capture the complexity of the process, thus necessitating the use of non-parametric methods. Finally, unlike Welch's estimator, the debiased Welch estimator does not require even spacing over frequency; we use this to demonstrate how we may simultaneously debias and compress the signal. We show this for a simulation of a stochastic process with log-linear decay in the power spectral density over frequency, a pertinent case-study for many applications. Code accompanies our results on multiple software platforms; both the R and python implementations are available at github.com/TIDE-ITRH.

2 Spectral analysis

2.1 Fundamentals and definitions

Define by $\{X_t\}$ a discrete real-valued stochastic process, sampled at interval Δ and indexed by $t \in \mathcal{Z}$, where $\mathcal{Z}$ is the set of integers. The process $\{X_t\}$ may be either thought of as a true discrete-time stochastic process, such as an auto-regressive model, or as uniformly sampled observations of a continuous-time stochastic process $\{X(t)\}$ in which case $X_t = X(\Delta t)$. We assume fourth-order stationarity, with finite fourth-order moments and absolutely continuous fourth-order cumulant spectrum, $\kappa(\alpha, \beta, \zeta)$. Define the auto-covariance sequence of $\{X_t\}$ as $\gamma(\tau) = \mathrm{E}[X_t X_{t-\tau}]$ for $\tau \in \mathcal{Z}$. Following Wiener–Khinchin's theorem, a necessary and sufficient condition for $\gamma(\tau)$ to be the auto-covariance function of $\{X_t\}$ is that there exists a power spectral distribution function $F(\omega)$ such that

$$\gamma(\tau) = \frac{1}{2\pi} \int_{-\pi/\Delta}^{\pi/\Delta} e^{i\omega\tau\Delta} \, \mathrm{d}F(\omega), \tag{1}$$

2

for $\omega \in [-\pi/\Delta, \pi/\Delta]$, where (1) is a Riemann-Stieltjes integral and ω is defined in radians. Absolute continuity of $\kappa(\alpha, \beta, \zeta)$ implies absolute summability in $\gamma(\tau)$. Consequently, there exists a uniformly continuous power spectral density (see, for instance, Section 4.2 Shumway and Stoffer, 2000), $f(\omega)$, such that $f(\omega)d\omega = dF(\omega)$, and $f(\omega)$ forms a Fourier pair with $\gamma(\tau)$ so that

$$\gamma(\tau) = \frac{1}{2\pi} \int_{-\pi/\Delta}^{\pi/\Delta} f(\omega)e^{i\omega\tau\Delta} \, d\omega, \quad f(\omega) = \Delta \sum_{\tau=-\infty}^{\infty} \gamma(\tau)e^{-i\omega\tau\Delta}. \tag{2}$$

As $f(\omega)$ is uniformly continuous over this interval, and according to the Vitali convergence theorem, $f(\omega)$ is Riemann integrable in ω.

Say we observe from $\{X_t\}$ an n-dimensional observation $X_n = (x_0, \ldots, x_{n-1})$. The most common estimator of $f(\omega)$ from X_n is the periodogram, $I_n(\omega)$, defined as the squared modulus of the discrete Fourier transform of X_n,

$$I_n(\omega) = |J_n(\omega)|^2, \quad J_n(\omega) = \Delta^{1/2} n^{-1/2} \sum_{t=0}^{n-1} x_t e^{-i\omega t\Delta}. \tag{3}$$

Alternatively, we may calculate the periodogram via the discrete Fourier transform of $\check{\gamma}(\tau)$, a biased estimator to $\gamma(\tau)$,

$$I_n(\omega) = \Delta \sum_{\tau=-n+1}^{n-1} \check{\gamma}(\tau)e^{-i\omega\tau\Delta}, \quad \check{\gamma}(\tau) = \frac{1}{n} \sum_{t=0}^{n-|\tau|-1} x_{t+|\tau|}x_t.$$

The periodogram is a biased and inconsistent estimator of $f(\omega)$. It has expectation $\mathrm{E}[I_n(\omega)] = f(\omega) * \mathcal{F}_n(\omega)$ where

$$\mathcal{F}_n(\omega) = \frac{\Delta}{2\pi n} \frac{\sin^2(n\omega\Delta/2)}{\sin^2(\omega\Delta/2)} \tag{4}$$

is the Fejér kernel, and variance $\mathrm{var}[I_n(\omega)] \approx f^2(\omega)$ which does not reduce with n, thus causing the inconsistency. The periodogram is asymptotically unbiased as $\mathcal{F}_n(\omega)$ tends to a Dirac delta function as $n \to \infty$. Often, practitioners will appeal to this to argue that the periodogram is a suitable estimator; however, the effects due to bias are related not only to n, but also to the dynamic range of $f(\omega)$. Even with massive n, for common $f(\omega)$ encountered in the sciences, the periodogram can be too biased to be useful (e.g. see the discussion in Thomson, 1982).

A standard technique to alleviate the bias in the periodogram is to apply a taper, or window, to the data. Tapering pre-multiplies the data with a taper to form the product $h_t X_t$ for $t = 0, \ldots, n-1$ where $\sum_{t=0}^{n-1} h_t^2 = 1$. The sequence $\{h_t\}$ is called the data taper. The tapered periodogram, otherwise known as the modified periodogram, is defined as

$$I_n(\omega; h) = |J_n(\omega; h)|^2, \quad J_n(\omega; h) = \Delta^{1/2} \sum_{t=0}^{n-1} h_t x_t e^{-i\omega t\Delta}.$$

The expectation of the tapered periodogram is $\mathrm{E}[I_n(\omega; h)] = f(\omega) * \mathcal{H}_n(\omega)$ where $\mathcal{H}_n(\omega)$ is the spectral window for $\{h_t\}$ defined by

$$\mathcal{H}_n(\omega) = \Delta \left| \sum_{t=0}^{n-1} h_t e^{-i\omega t\Delta} \right|^2.$$

Tapering can be effective in removing bias; however, it is not a panacea. The data taper is generally chosen so as to reduce bias in the form of broadband blurring in $I_n(\omega; h)$; this comes with the trade-off

that bias from narrowband blurring is increased. Further, tapering, in effect, reduces the amount of data and so the tapered periodogram has a higher variance as compared to the standard periodogram. This variance can be reduced by applying multiple tapers (multi-tapering), but this then reintroduces bias such that the level of the bias-variance trade-off must be in practice controlled by the practitioner. Setting $h_t = n^{-1/2}$ recovers the periodogram as $\mathcal{H}_n(\omega) = \mathcal{F}_n(\omega)$. For this reason all periodograms may be considered to be tapered, and so we will use the notation $I_n(\omega; h)$ to refer to both tapered and standard periodograms throughout.

2.2 Debiased parametric estimation

Rather than using $I_n(\omega; h)$ as a direct estimate to $f(\omega)$, it is common to instead use $I_n(\omega; h)$ to fit some parametric form $f(\omega; \vartheta)$, with Fourier pair $\gamma(\omega; \vartheta)$. To avoid the unwieldy computation often associated with time-domain methods requiring matrix inversion, it is standard to approximate the exact maximum likelihood with a discretized form of the Whittle likelihood

$$l_{\mathrm{W}}(\vartheta) = - \sum_{\omega \in \Omega_n} \left(\log f(\omega; \vartheta) + \frac{I_n(\omega; h)}{f(\omega; \vartheta)} \right), \tag{5}$$

where $\Omega_n = 2\pi(\Delta n)^{-1}(-\lfloor n/2 \rfloor, \ldots, -1, 0, 1, \ldots, \lceil n/2 \rceil - 1)$ is the set of Fourier frequencies for an observed stochastic process of length n. Due to the inherent bias in $I_n(\omega; h)$, parameter estimation from using (5) can be biased (for example, see Dahlhaus, 1988). Sykulski et al. (2019) proposed a solution to this problem, whereby the pseudolikelihood

$$l_{\mathrm{D}}(\vartheta) = - \sum_{\omega \in \Omega_n} \left(\log \check{f}_n(\omega; \vartheta) + \frac{I_n(\omega; h)}{\check{f}_n(\omega; \vartheta)} \right) \tag{6}$$

is defined. Here, we substitute $\check{f}_n(\omega; \vartheta) = E[I_n(\omega; h)] = f(\omega; \vartheta) * \mathcal{H}_n(\omega)$ for $f(\omega; \vartheta)$ in (5). We use the caron diacritic throughout this manuscript to indicate intentionally biased quantities. Sykulski et al. (2019) further showed that the convolution $f(\omega; \vartheta) * \mathcal{H}_n(\omega)$ can be efficiently calculated as

$$\check{f}_n(\omega; \vartheta) = 2\Delta \times \mathrm{Re} \left\{ \sum_{\tau=0}^{n-1} \left(\sum_{t=0}^{n-\tau-1} h_t h_{t+\tau} \right) \gamma(\tau; \vartheta) e^{-i\omega\tau\Delta} \right\} - \Delta \times \gamma(0; \vartheta) \tag{7}$$

using fast Fourier transforms. When $h_t = n^{-1/2}$, and so $I_n(\omega; h)$ is the periodogram, $\sum_{t=0}^{n-\tau-1} h_t h_{t+\tau} = 1 - \tau/n$, and (7) is the standard form for the debiased Whittle likelihood as presented in Equation (9) of Sykulski et al. (2019). This technique debiases estimates of ϑ, and hence $f(\omega; \vartheta)$ and $\gamma(\omega; \vartheta)$, in parametric estimation.

2.3 Welch's method for spectral density estimation

Welch's method segments a time series $x_0, \ldots, x_{n-1}$ into M partitioned or overlapping blocks of length L, and applies a length L data taper to each block. We define the periodogram of the mth block, for $m = 0, \ldots, M-1$, as

$$I_L^m(\omega; h) = \Delta \left| \sum_{t=0}^{L-1} h_t x_{(t+mS)} e^{-i\omega t\Delta} \right|^2,$$

where S is an integer-valued shift factor satisfying $0 < S \leq L$, so that $p = (L-S)/L$ is the percentage overlap of the blocks, and the relationship between M, L and p is

$$ML(1-p) + Lp = n, \tag{8}$$

4

such that setting two of $\{M, L, p\}$ fixes the third for a given n. Welch's estimator is defined as

$$\bar{I}_L(\omega; h) = \frac{1}{M} \sum_{m=0}^{M-1} I_L^m(\omega; h). \tag{9}$$

The degree of overlap, p, and the choice of data taper, $\{h_t\}$, are modelling choices often informed by either desired properties of the analysis or preferences within scientific disciplines. For instance, it is standard in the engineering sciences to assume a 50% overlap ($p = 0.5$) with a Hamming taper: see the MATLAB documentation of the function pwelch. Welch's estimator has expectation $\mathrm{E}[\bar{I}_L(\omega; h)] = f(\omega) * \mathcal{H}_L(\omega)$ and variance

$$\mathrm{var}\left[\bar{I}_L(\omega; h)\right] = \frac{1}{M^2} \sum_{m=0}^{M-1} \mathrm{var}\left[I_L^m(\omega; h)\right] + \frac{2}{M^2} \sum_{m<m'} \mathrm{cov}\left[I_L^m(\omega; h), I_L^{m'}(\omega; h)\right]$$

$$= \frac{\mathrm{var}[I_L(\omega; h)]}{M}\left(1 + \frac{2}{M} \sum_{m<m'} \rho(\omega; |m-m'|, h)\right), \tag{10}$$

where $\rho(\omega; |m-m'|, h) = \mathrm{cor}\left[I_L^m(\omega; h), I_L^{m'}(\omega; h)\right]$ and $\mathrm{var}[I_L(\omega; h)] = \mathrm{var}[I_L^m(\omega; h)]$ for all m. We establish some important properties of Welch's estimator in Theorem 1.

Theorem 1. *Assume a fourth-order stationary stochastic process $\{X_t\}$ with finite fourth-order moments and absolutely continuous fourth-order cumulant spectrum. Welch's estimator, defined in (9), of the observed process $\mathrm{X}_n = (x_0, \ldots, x_{n-1})$, with data taper $\{h_t\}$ that satisfies $\sum h_t^2 = 1$, has the following properties.*

  a) The estimator, $\bar{I}_L(\omega; h)$, satisfies $\bar{I}_L(\omega; h) = f(\omega) * \mathcal{H}_L(\omega) + \mathcal{O}_p(M^{-1/2})$.

  b) The variance $\mathrm{var}[\bar{I}_L(\omega; h)]$ converges asymptotically, in L, to

$$\lim_{L \to \infty} \mathrm{var}[\bar{I}_L(\omega; h)] = c \, \mathrm{var}[I_L(\omega; h)]$$

  for all $\omega \neq 0, \omega_{\mathcal{N}}$. Here, c is a constant of proportionality that is constant over ω, and $\omega_{\mathcal{N}}$ denotes the Nyquist frequency.

  c) The quantity $M^{-1/2} \bar{I}_L(\omega; h)$ tends to a Gaussian distribution as $M \to \infty$.

Proof. Proofs are provided in the Supplementary Material.

Remark 1. *As n increases, then it is not possible to increase both L, the block length, and M, the number of blocks, linearly with n for a fixed overlap p, see (8); a trade-off is required. For fixed L and linearly increasing M, Theorem 1a establishes that Welch's estimate has the optimal convergence rate of $\mathcal{O}_p(M^{-1/2}) = \mathcal{O}_p(n^{-1/2})$, but the estimator is inconsistent for all processes except white noise due to the bias inherent in $f(\omega) * \mathcal{H}_L(\omega)$ for fixed L as discussed. On the other extreme, for fixed M and linearly increasing L, the bias asymptotically vanishes but the variance is $\mathcal{O}_p(1)$ (Theorem 1a) and therefore the Welch estimate suffers the same inconsistency as the periodogram (Theorem 1b). Consistency is only achieved by increasing both L and M with n at reduced rates.*

3   Debiasing Welch's Method

3.1   Constructing biased bases

To construct a debiased and consistent estimate to $f(\omega)$ based on Welch's method, we use concepts proposed by Sykulski et al. (2019) but extend them to a non-parametric setting. Specifically, here we

construct from a family of bases $B_k(\omega)$, a family of biased bases $\check{B}_k(\omega)$. We assume the functional form $f(\omega; \vartheta) = \sum_{k=1}^{K} a_k B_k(\omega)$ and set $\check{f}(\omega; \vartheta) = \sum_{k=1}^{K} a_k \check{B}_k(\omega)$ in (6) to provide debiased inference for the parameters $\vartheta = (a_1, \ldots, a_K)$. Here, the $B_k(\omega)$ are basis functions specified from some family of bases chosen to represent some desirable property of $f(\omega)$. We set $\int_{-\infty}^{\infty} B_k(\omega) d\omega = 1$. Due to the linearity of the integral in (2), assuming $f(\omega; \vartheta) = \sum_{k=1}^{K} a_k B_k(\omega)$ implies $\gamma(\tau; \vartheta) = \sum_{k=1}^{K} a_k \rho_k(\tau)$ where each $\rho_k(\tau)$ are the auto-correlation functions calculated from $B_k(\omega)$ as

$$\rho_k(\tau) = \frac{1}{2\pi} \int_{-\pi/\Delta}^{\pi/\Delta} B_k(\omega) e^{i\omega\tau\Delta} d\omega. \tag{11}$$

Due to the distributivity of the convolution operator the expected periodogram is $\check{f}(\omega; \vartheta, h) = \mathrm{E}[I_n(\omega; h)] = \sum_{k=1}^{K} a_k \check{B}_k(\omega; h)$ where each $\check{B}_k(\omega; h)$ is calculated exactly using a fast Fourier transform by substituting $\rho_k(\tau)$ for $\gamma(\tau; \vartheta)$ in (7).

3.2 A Riemann approximation to the spectral density

Section 3.1 describes a general approach to bias any basis family. Here, we provide specific details with respect to a Riemannian approximation of $f(\omega)$. As $f(\omega)$ is Riemann integrable then we may approximate $f(\omega)$ by summating contiguous rectangular functions; this approximation becomes exact as the width of the rectangular functions tends to zero. Define the rectangular function by

$$\mathrm{rect}(\omega) = \begin{cases} 1 & |\omega| < 1/2 \\ 1/2 & |\omega| = 1/2 \\ 0 & \text{elsewhere} \end{cases}$$

and the symmetric rectangular function with centre ω^c and width δ as

$$\mathrm{symrect}(\omega; \omega^c, \delta) = \mathrm{rect}\left(\frac{\omega - \omega^c}{\delta}\right) + \mathrm{rect}\left(\frac{\omega + \omega^c}{\delta}\right), \tag{12}$$

for $\omega^c \geq \delta/2$. As we are concerned with real-valued time series, $f(\omega) = f(-\omega)$. Define $(\omega_0, \omega_1, \ldots, \omega_K)$ as a partition of $[0, \omega_{\mathcal{N}}]$. The mid-point Riemann approximation to $f(\omega)$ is

$$f(\omega) \approx \sum_{k=1}^{K} f(\omega_k^c) \, \mathrm{symrect}(\omega; \omega_k^c, \delta_k), \quad \omega \in [-\pi/\Delta, \pi/\Delta], \tag{13}$$

with centres $\omega_k^c = \omega_{k-1} + \delta_k/2$ and widths $\delta_k = \omega_k - \omega_{k-1}$. The approximation in (13) converges to equality as $K \to \infty$ and all $\delta_k \to 0$. This approach does not require us to space the bases regularly; any partition can be defined, allowing for irregularly spaced bases. For now, so as to mimic the behaviour of Welch's estimate, we assume the bases to be regularly spaced in ω, and so $\delta_k = \delta$ for all k. We define the centres and widths of the symmetric rectangular functions so that for a maximum value of $K = \lceil (L-1)/2 \rceil$, $\omega_k^c = k\delta - \delta/2$ and $\delta = \pi/(\Delta K)$. Setting $B_k(\omega) = \mathrm{symrect}(\omega; \omega_k^c, \delta)$, and following the results of Tobar (2019), we calculate via (11)

$$\rho_k(\tau; \omega_k^c, \delta) = \delta^{-1} \mathrm{sinc}(\tau\delta) \cos(\omega_k^c \tau), \tag{14}$$

where $\mathrm{sinc}(\tau) = (\pi\tau)^{-1} \sin(\pi\tau)$ and $\mathrm{sinc}(0) = 1$. To calculate $\check{B}_k(\omega; h)$ we substitute $\rho_k(\tau; \omega_k^c, \delta)$ in (7).

6

3.3 Model fitting

For a given choice of bases $B_k(\omega)$ the final step is to estimate $\vartheta = (a_1, ..., a_k)$ to recover the spectral estimate $f(\omega; \vartheta) = \sum_{k=1}^{K} a_k B_k(\omega)$. The preferred debiased approach would be to specify $\check{f}(\omega; \vartheta) = \sum_{k=1}^{K} a_k \check{B}_k(\omega; h)$ and solve for the a_k by maximising the debiased Whittle likelihood defined in (6). For the approximation to $f(\omega)$ in (13) to be reasonable, however, we are required to define a potentially large number of bases, K, and so it is likely that maximising (6) is computationally infeasible using naive optimisation routines.

To proceed we observe from Theorem 1c that $\bar{I}_L(\omega; h)$ converges, with M, to be Gaussian, and so we model $\bar{I}_L(\omega; h) = \sum_{k=1}^{K} a_k \check{B}_k(\omega; h) + \epsilon(\omega)$, for heteroskedastic and Gaussian $\epsilon(\omega)$ with $\text{var}[\epsilon(\omega)] = \text{var}[\bar{I}_L(\omega; h)]$. Define the vector $\check{B}(\omega; h) = (\check{B}_1(\omega; h), \dots, \check{B}_K(\omega; h))$ as the column vector of all the biased bases at ω. Weighted least squares can be used to estimate a solution of the form

$$\arg\min_{\vartheta} \sum_{\omega \in \Omega_L} \left\{ \text{var}[\bar{I}_L(\omega; h)]^{-1} \left(\bar{I}_L(\omega; h) - \vartheta^{\mathrm{T}} \check{B}(\omega; h) \right)^2 \right\}. \tag{15}$$

As $\text{var}[\bar{I}_L(\omega; h)]$ is dependent on $f(\omega)$, the true power spectral density we are trying to estimate, the solution to (15) is not analytical. As an approximation to (15), we substitute $\bar{I}_L(\omega; h)^2$ for $\text{var}[\bar{I}_L(\omega; h)]$ and instead solve

$$\hat{\vartheta} = \arg\min_{\vartheta} \sum_{\omega \in \Omega_L} \left\{ \bar{I}_L(\omega; h)^{-2} \left(\bar{I}_L(\omega; h) - \vartheta^{\mathrm{T}} \check{B}(\omega; h) \right)^2 \right\}. \tag{16}$$

The motivation for (16) is as follows. From Theorem 1b, as $\lim_{L \to \infty} \text{var}\left[\bar{I}_L(\omega; h) \right] = c \, \text{var}\left[I_L(\omega; h) \right]$, over all ω, we substitute $\text{var}\left[I_L(\omega; h) \right]$ for $\text{var}\left[\bar{I}_L(\omega; h) \right]$ in (15). Further, as we establish in Theorem 2 below, $\bar{I}_L(\omega; h)^2$ converges in M and L to $\text{var}[I_L(\omega; h)]$, and so we approximate $\text{var}[I_L(\omega; h)]$ by $\bar{I}_L(\omega; h)^2$, resulting in (16). From $\hat{\vartheta} = (\hat{a}_1, \dots, \hat{a}_K)$, we define a debiased functional estimate of $f(\omega)$ as $f(\omega; \hat{\vartheta}) = \sum_{k=1}^{K} \hat{a}_k B_k(\omega)$. For the symmetric rectangular basis function of Section 3.2, we define the debiased Welch estimator at a discrete set of frequencies as $\hat{I}(\omega_k) = \hat{a}_k B_k(\omega_k) = \hat{a}_k / \delta_k$ for $\omega_k \in \{\omega_1^c, \dots, \omega_K^c\}$; this is analogous to the frequencies for which Welch's estimator is generally defined.

Theorem 2. *Assume a fourth-order stationary process, $\{X_t\}$, with finite fourth-order moments and absolutely continuous fourth-order cumulant spectrum, $\kappa(\alpha, \beta, \zeta)$. The variance of the periodogram of any observed length-L segment of $\mathrm{X}_n = (x_0, \dots, x_{n-1})$, for all $\omega \neq 0, \omega_{\mathcal{N}}$, and with data taper $\{h_t\}$ that satisfies $\sum h_t^2 = 1$, is*

a) $\text{var}[I_L(\omega; h)] = \bar{I}_L(\omega; h)^2 + \mathcal{O}_p \left(\frac{1}{\sqrt{M}} + \frac{\log^2 L}{L^2} \right)$, *when $\kappa(\alpha, \beta, \zeta) = 0$ for all α, β, ζ; and*

b) $\text{var}[I_L(\omega; h)] = \bar{I}_L(\omega; h)^2 + \mathcal{O}_p \left(\frac{1}{\sqrt{M}} + \frac{1}{L} \right)$, *otherwise.*

Proof. The proof is provided in the Supplementary Material.

Remark 2. *From Theorem 1 of Sykulski et al. (2019), we find that the debiased Welch estimator, $\hat{I}(\omega_k)$, when computed through (6), is unbiased so that $\mathrm{E}[\hat{I}(\omega_k)] = f(\omega_k; \vartheta)$. The weighted least squares routine in (16) follows asymptotic arguments in Theorems 1 and 2 that result in an estimator that is asymptotically unbiased and $\mathcal{O}_p(M^{-1/2})$ as long as L and M both increase with n, and significantly debiased for finite samples compared to the standard Welch estimator, as we will demonstrate in the following sections through simulation and applications.*

3.4 Computation

We summarize the computation of the debiased Welch estimator in Algorithm 1 in the Supplementary Material, with two variants provided. The first variant, shown in lines 3–8 of Algorithm 1, provides the option to space the K bases evenly or unevenly over frequency. Even spacing of the bases provides a closer analogue to Welch's estimator; here, the choice of integer valued $K \leq \lceil (L-1)/2 \rceil$ is the only additional user decision required by the debiased Welch estimator. When there is large bias present in Welch's estimator, choosing K close to $\lceil (L-1)/2 \rceil$ can lead to an ill-defined solution. In general, we recommend $K = \lceil (L-1)/4 \rceil$ as a good initial estimate which, in effect down-samples the Fourier frequencies by an order of two. For uneven spacing, the centres and widths are all user-specified. We discuss uneven spacing further in Section 6 with an example provided for high-frequency slope estimation. The second variant of the model, shown in lines 12–15 of Algorithm 1, provides an option to impose non-negativity on ϑ in (16), constraining the solution space to $\hat{\vartheta} \in \mathcal{R}^+$. The debiased Welch estimator is not guaranteed to yield a non-negative solution; due to finite sampling error, small negative values may result. This is particularly so when the choice of K is too high and so the solution to the linear system in (16) is unstable. Efficiently computing non-negative least-squares estimates has been long understood; in the accompanying code we implement results from Lawson and Hanson (1974).

The computational order of the debiased Welch estimator, for both even and uneven spacing, is $\mathcal{O}(\max\{n \log L, K^3\})$. Here, the first term is the computational order of Welch's estimator, and the second term is the computational order to do the debiasing in (16). The number of bases K scales with L and so $\mathcal{O}(K^3) \propto \mathcal{O}(L^3)$ for even spacing. From Theorem 2, we observe that the optimal rate with which to scale L with n is at maximum $n^{1/3}$, and so the debiasing in (16) scales at most $\mathcal{O}(n)$. Thus, the debiased Welch estimator retains the same computational order of the standard Welch estimator, $\mathcal{O}(n \log L)$.

4 Simulations of autoregressive processes

To test empirical performance of the debiased Welch estimator, we run a simulation study using a canonical model for biased spectral density estimation: the AR(4) model of Percival et al. (1993). The model is specified as $X_t = \sum_{j=1}^{4} \phi_j X_{t-j} + \epsilon_t$ where $\epsilon_t \sim \mathcal{N}(0, \sigma^2)$ and $\{\phi_1, \phi_2, \phi_3, \phi_4, \sigma\} = \{2.7607, -3.8106, 2.6535, -0.9238, 1\}$. To show units in subsequent plots, we measure $\{X_t\}$ in metres, t in seconds and assume $\Delta = 1$. Throughout, we calculate standard periodograms, corresponding to $h_t = L^{-1/2}$. Similar results with other tapers were found, with the bias in Welch's estimator being reduced but not eliminated. First, we plot in Figure 1 the standard (left) and debiased (right) Welch estimates with black solid lines, calculated from a single realisation from the AR(4) model. We generate a time series of length $32,768$ (2^{15}) and set $M = 64$ (2^6) and $L = 512$ (2^9) with zero overlap for both estimates. In both plots, the true spectral density is shown by the dashed grey line, and the expected value of Welch's estimator, calculated from (7) using the auto-covariance function of the AR(4) model, is shown by the solid grey line. Visually, the debiased Welch estimate provides a closer estimate of the true spectral density, especially in regions of low power where we know the bias to be significant.

We now explore how the bias, standard deviation and root-mean-square error of the Welch estimators behave as a function of M for fixed L. For each $M \in \{8, 16, 32, 64, 128, 256\}$ and $p \in \{0, 0.5\}$ we generate 1000 random time series from the AR(4) model with fixed segment length $L = 1024$ (2^{10}). For each M and p, we calculate, over the ensemble, the empirical mean absolute bias, standard deviation, and root-mean-square error, at each frequency. We aggregate the scores by computing the mean log value across frequency and for each metric; this makes the error process of the metrics independent of the expected power at each frequency and hence aggregates the frequencies with equal importance. Results are shown in Figure 2. The dashed lines show the results from the Welch estimator, the solid lines from the debiased Welch estimator, the grey lines with an overlap of $p = 0.5$ and the black lines with an overlap of $p = 0$. The results of this simulation study support a number of our theoretical claims. The
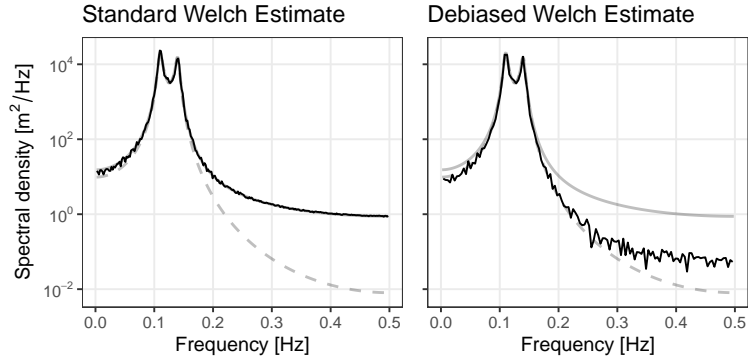
Figure 1: Welch estimates of an AR(4) random time series. The AR(4) model is defined formally in the text; the true spectral density is shown by the dashed grey line and the expected Welch estimate is shown by the solid grey line. The Welch estimates are shown by solid black lines with the standard Welch estimate shown left, and the debiased Welch estimate shown right.

black dot-dashed line shows the $M^{-1/2}$ convergence rate which is consistent with the theory established in Theorem 1a for the Welch estimator, and is maintained for the debiased Welch estimator. The absolute bias tends to zero for the debiased Welch estimator as the approximation in Theorem 2 improves with increasing M, justifying the computation of the debiased Welch estimates using (16). The absolute bias does not converge to zero for the standard Welch estimator due to the finite-sample bias of periodograms of fixed length L as already established in Theorem 1a.

Finally, we examine the performance of the Welch estimators as a function of L, for fixed M. Similarly to before, we generate 1000 random time series, but with fixed $M = 64$ and $L \in \{512, 1024, 2048\}$, all with zero overlap. We calculate three metrics over frequency, for each time series: the root-mean-squared-error; the root-mean-squared-log-error, that is, the root-mean-squared-error calculated over the log values; and the mean-absolute-percentage-error. The results are summarized in Table 1 by the mean values and standard deviation, in brackets, calculated over the ensemble. Root-mean-squared-error is largely determined by the higher power regions in the spectral estimates. In these regions we do not expect much deviation between the estimators, as bias due to blurring predominately occurs in the low power regions. This is reflected in the results where both Welch estimators have similar root-mean-squared-error values across all L. Conversely, the root-mean-squared-log-error is power normalising, that is, the performance of the spectral estimates is calculated evenly across all frequencies, regardless of the spectral density. Here, we see a clear increase in performance by the debiased Welch estimator across all simulations with highly significant separation between the scores. This is also reflected in the mean-absolute-percentage-error, a metric commonly used in evaluating spectral density estimation (see

Table 1: Metrics calculated over an ensemble of 1000 members for fixed M and varying L.

	$L = 512$		$L = 1024$		$L = 2048$	
	Welch	D.Welch	Welch	D.Welch	Welch	D.Welch
RMSE	17 (13)	19(15)	12 (9.8)	13 (10)	8.8 (6.7)	9.2 (6.9)
RMSLE	17 (1.6)	3.1 (2.5)	9.9 (1.2)	1.8 (1.4)	5.6 (0.76)	1.0 (0.74)
MAPE	64 (8.6)	13 (4.3)	34 (4.5)	9.5 (1.8)	19 (2.3)	8.1 (0.67)

RMSE, Root Mean Squared Error; RMSLE, Root Mean Squared Log Error; MAPE, Mean Absolute Percentage Error.
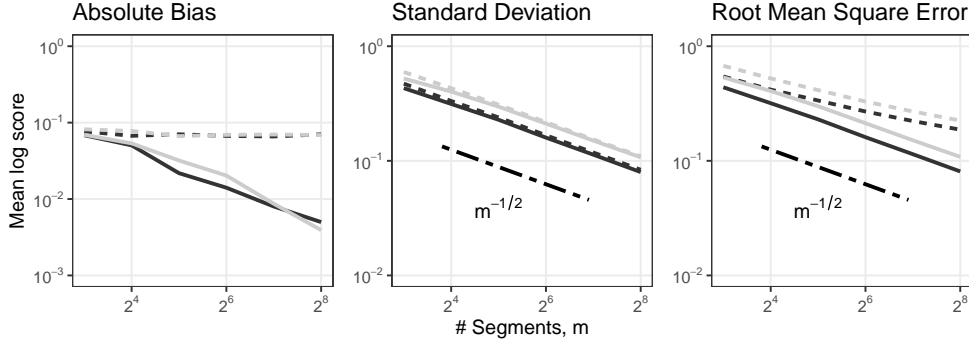
9

Figure 2: Empirical bias, standard deviation and root mean squared error of the standard and debiased Welch estimates over M, for fixed L. Each data point represents the metrics calculated over an 1000 member ensemble for each frequency and the aggregated by the mean log values. The dashed lines represent the Welch estimates, the solid lines the debiased Welch estimates, the grey lines with an overlap of 0.5 and the black lines with an overlap of 0.

Percival et al., 1993).

5   Application to coastal wave monitoring

We now demonstrate the use of the debiased Welch estimator applied to a measured data-set of coastal sea-surface heights. The data are measured from two locations with differing mean water depths on the Southern coast of Western Australia: Ocean Beach and Torbay. Contemporaneous measurements of sea-surface height are taken from acoustic and pressure sensors. Acoustic sensors provide measurements of the true process via acoustic ranging and pressure sensors measure pressure variation on the sea-bed and translate this to a measurement of sea surface height. Shallow water wave theory states that pressure is attenuated through depth as

$$\Lambda_p(z; k) = \frac{\cosh(k(d + z))}{\cosh(kd)}, \tag{17}$$

where d is the undisturbed depth, $-z$ is depth from the sea-surface to the sensor and, here, k is wavenumber. We can also define (17) as a function of frequency using the dispersion relation (Dean and Dalrymple, 1991). We show two 5-minute chunks of the measured time series from both sites on the left of Figure 3; the solid grey and dashed black lines are measurements from the acoustic and pressure sensors, respectively. On the right of Figure 3 we show the attenuation of the pressure signal over frequency. The high frequency signal in the Torbay measurements see larger attenuation than in the Ocean Beach measurements due to the deeper mean water level. Due to the attenuation of the high frequency signal, in both records, we expect a high dynamic range in the pressure signal, and hence non-ignorable spectral bias due to blurring.

We calculate power spectral density estimates of a three-hour record of sea-surface heights at each location; the results are shown in Figure 4. First, we calculate the Welch estimates, shown in the left hand panels. Here, the grey and black lines are from the acoustic measurements, respectively. As expected, there is good agreement between the estimators at low frequencies, and the pressure signal is attenuated at higher frequencies. The spectral shape of the Ocean Beach record is interesting: there are two spectral peaks around 0.06 Hz and 0.12 Hz, implying the presence of both a well formed swell (low-frequency) and wind-sea (high-frequency), likely due to a local storm. This behaviour is hard to capture parametri-
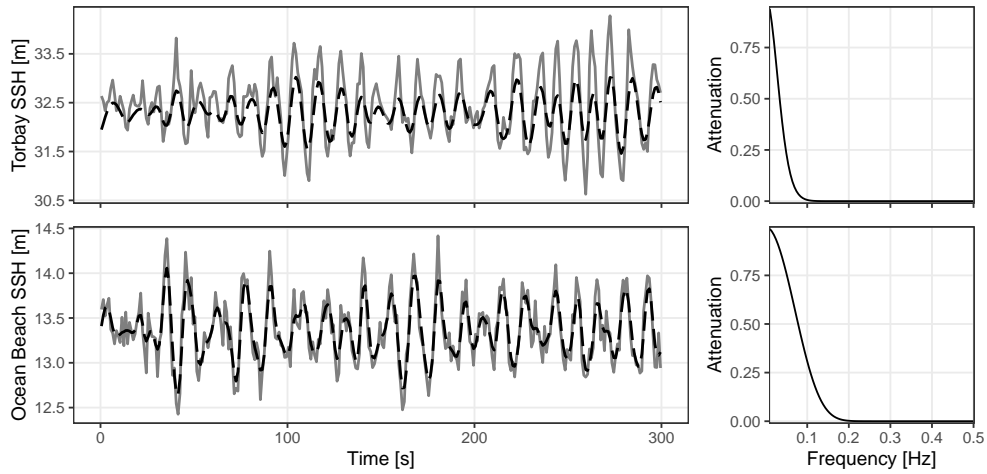
10

Figure 3: Contemporaneous measurements of sea-surface height from acoustic (grey) and pressure (black-dashed) sensors, measured in Western Australia at Torbay (top) and Oean Beach (bottom). The right hand plots show the attenuation of the pressure signal over frequency and are dependent on the mean water depths.
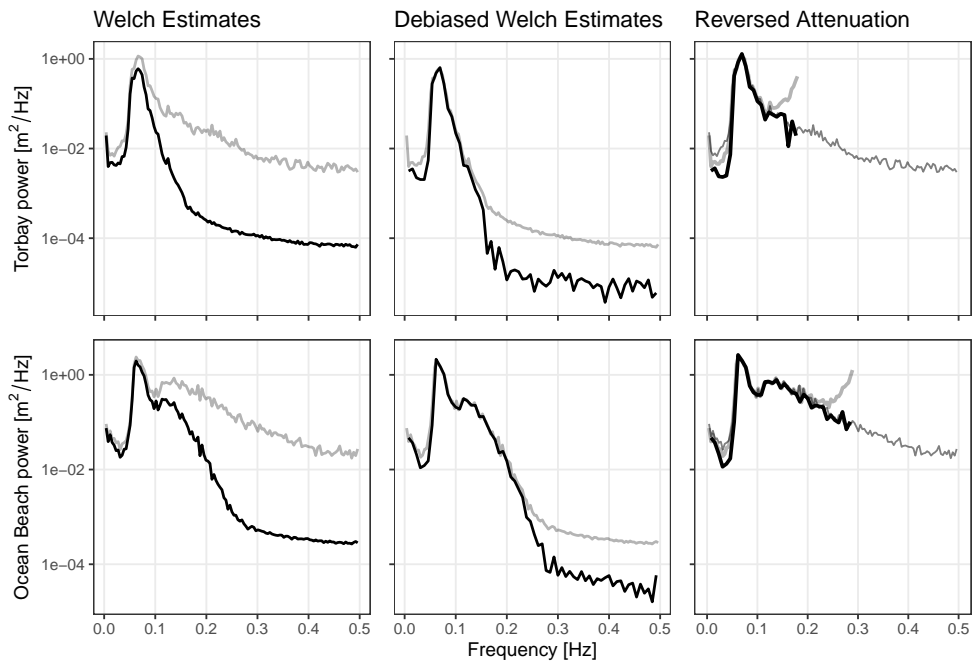

Figure 4: Welch estimates of sea-surface height spectra from acoustic and pressure sensors located at Torbay (top) and Ocean Beach (bottom). The left plots show the standard Welch estimates of the acoustic (grey) and pressure (black) measurements. The middle plots show the debiased Welch estimate of the pressure data (black) and, for comparison, the Welch estimate (grey). The right plots show the standard (grey) and debiased (black) Welch estimates of the pressure measurements inverted through the attenuation function. The thin grey line is the acoustic signal used as a notion of ground truth.

11

cally and is a good example to motivate the use of non-parametric methods. The black lines in the middle plots are the debiased Welch estimates calculated from the pressure signal, and the grey lines are the Welch estimates, for reference. We do not display the debiased estimate for the acoustic signal as the bias correction is very small here due to the small dynamic range. Finally, the right hand plot shows the Welch estimates of the pressure measurements inverted through the attenuation function to give an estimate of the true wave power spectra; the thick grey and black lines show the inverted Welch and debiased Welch estimates, respectively. These estimates are not shown above 0.18 Hz and 0.28 Hz for Torbay and Ocean Beach, respectively, as this is where the noise floor of the pressure sensor dominates the signal. The thin grey line is the acoustic Welch estimate, also shown in the left hand plots, and is used for a notion of the ground truth. Due to in-situ pre-processing of the pressure signal, whereby the signal is demeaned of tidal effects, there is some bias between the two signals at low-frequencies below 0.05 Hz across the entire data-set. Overall, the debiased Welch estimator gives a better estimate to the true process over broader range of frequencies. As compared to pressure sensors, acoustic sensors are more expensive, and due to larger power requirements, do not allow for long field deployments. Increasing the signal extraction from pressure sensors motivates an increase in use which will, in turn, enable cheaper and longer measurement campaigns.

6 Unevenly spaced bases for signal compression

To be analogous to Welch's estimator, in Section 3 we define the debiased Welch estimator with even basis spacing over frequency. As noted therein, we do not require this, and can alternatively define the bases by an irregular partition over frequency. For spectra whose value varies slowly over certain neighbourhoods of frequency, we argue that a wider basis spacing would lead to little reduction of accuracy in estimating the true process. Allowing for wider, and irregularly spaced bases serves two purposes: first we achieve a degree of signal compression, as compared to the Welch estimator; and second, we reduce the variance of the estimator as there are more data informing the coefficient of each basis. The code provided alongside this manuscript accepts uneven bases by providing the ω_k^c and δ_k, as defined in (13), as user defined inputs for all k.

To demonstrate this concept, we calculate Welch and debiased Welch estimates of a random sample from a Matérn process parameterized as

$$\gamma(\tau) = \frac{2\sigma^2}{\Gamma(\alpha - 1/2)2^{\alpha - 1/2}}|\tau|^{\alpha - 1/2}\kappa_{\alpha - 1/2}(|\tau|), \quad f(\omega) = \frac{\sigma^2}{(\omega^2 + \lambda^2)^\alpha},$$

with $\sigma = 1$, $\lambda = 0.1$ and $\alpha = 11/6$, where $\Gamma(\cdot)$ denotes the gamma function and $\kappa_{\alpha - 1/2}(\cdot)$ the order $\alpha - 1/2$ modified Bessel function of the second kind. The true power spectral density and the expected value of Welch's estimator for the Matérn process are shown in the plots in Figure 5 by the dashed and solid grey lines, respectively. The Matérn power spectral density is asymptotically, in ω, log-linear and so we space the bases of the debiased Welch estimator evenly in log-frequency. The location of the bin-centres, ω_k^c, are shown by the rug-plot on the frequency axes in Figure 5. Asymptotically log-linear processes are common in many sciences, for example, background ocean spectra and turbulent dissipation in oceanography (Garrett and Munk, 1972; Zulberti et al., 2022), stellar rotation periods and red-shift in astronomy (Foreman-Mackey et al., 2017) and long-memory processes (Palma, 2007), and so this example provides a useful case-study to many applied fields. We sample a length $32,768$ (2^{15}) time series with $\Delta = 1$ and calculate the Welch estimate, with parameters $M = 32$ (2^5), $L = 1024$ (2^{10}) and no overlap, shown in the left plots of Figure 5 in black. The debiased Welch estimate, with log-spaced bases, is calculated and shown in the right plots of Figure 5 in black. The bottom plots of Figure 5 are identical to the top, except with frequency shown on a log scale. Not only do we reduce empirical bias in the estimate, we also compress the signal by a factor of ~ 50 and reduce the standard deviation of the estimate from the true spectral density.
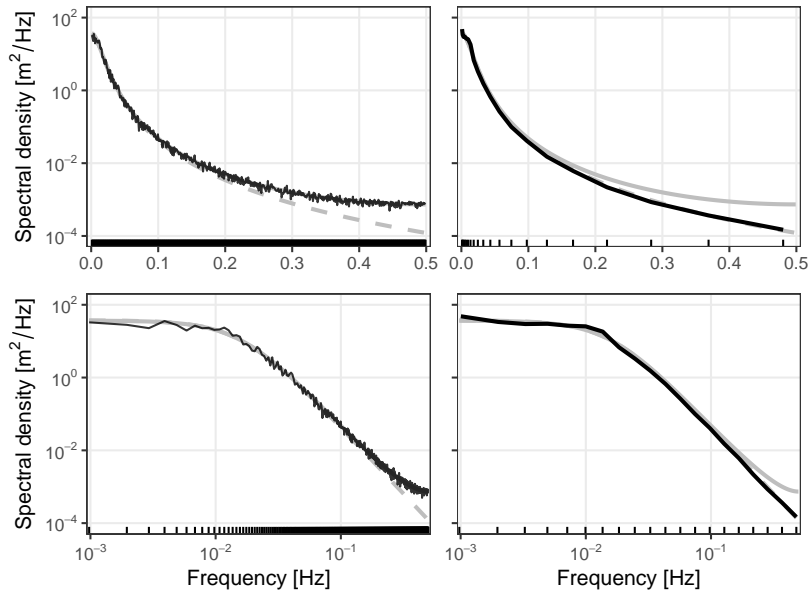
Figure 5: Welch estimates of a Matérn power spectrum with uneven basis spacing. The top plots show frequency on a linear scale and the bottom plots on a log scale. The standard Welch estimate is shown left and debiased Welch estimate, with uneven basis spacing, is shown right with black solid lines. Locations of the Fourier frequencies and basis centres for the Welch and debiased Welch estimates are shown by the rug plots on the frequency axes. In all plots, the true power spectral distribution and expected Welch estimate are shown by the dashed and solid grey lines, respectively.

Acknowledgement

References

Anderson, T.W., 1971. The statistical analysis of time series. John Wiley & Sons.

Brillinger, D.R., 1975. Time series: data analysis and theory. Holt, Rinehart and Winston Inc.

Dahlhaus, R., 1988. Small sample effects in time series analysis: a new asymptotic theory and a new estimate. The Annals of Statistics , 808–841.

Dean, R.G., Dalrymple, R.A., 1991. Water wave mechanics for engineers and scientists. volume 2 of *Advanced Series on Ocean Engineering*. World Scientific Publishing Co Pte Ltd.

Foreman-Mackey, D., Agol, E., Ambikasaran, S., Angus, R., 2017. Fast and scalable Gaussian process modeling with applications to astronomical time series. The Astronomical Journal 154, 220.

Garrett, C., Munk, W., 1972. Space-time scales of internal waves. Geophysical Fluid Dynamics 3, 225–264.

Katznelson, Y., 1968. An introduction to harmonic analysis. John Wiley & Sons, Inc.

Lawson, C.L., Hanson, R.J., 1974. Solving least squares problems. Prentice Hall.

Palma, W., 2007. Long-memory time series: theory and methods. John Wiley & Sons.

Percival, D.B., Walden, A.T., et al., 1993. Spectral analysis for physical applications. Cambridge University Press.

Shumway, R.H., Stoffer, D.S., 2000. Time series analysis and its applications. volume 3. Springer.

Sykulski, A.M., Olhede, S.C., Guillaumin, A.P., Lilly, J.M., Early, J.J., 2019. The debiased Whittle likelihood. Biometrika 106, 251–266.

Thomson, D.J., 1982. Spectrum estimation and harmonic analysis. Proceedings of the IEEE 70, 1055–1096.

Tobar, F., 2019. Band-limited Gaussian processes: The sinc kernel. Advances in Neural Information Processing Systems 32.

Welch, P., 1967. The use of fast Fourier transform for the estimation of power spectra: a method based on time averaging over short, modified periodograms. IEEE Transactions on audio and electroacoustics 15, 70–73.

Zulberti, A., Jones, N., Rayson, M., Ivey, G., 2022. Mean and turbulent characteristics of a bottom mixing-layer forced by a strong surface tide and large amplitude internal waves. Journal of Geophysical Research: Oceans 127, e2020JC017055.